Int. J. Heat Mass Transfer. Vol. 30, No. 4, pp. 613–622, 1987
Printed in Great Britain

0017–9310/87 $3.00 + 0.00
Pergamon Journals Ltd.

Melting in a vertical tube rotating about a vertical, colinear axis

A. CHABOKI and E. M. SPARROW
Department of Mechanical Engineering, University of Minnesota, Minneapolis, MN 55455, U.S.A.

(*Received* 30 *April* 1986 *and in final form* 18 *August* 1986)

Abstract—Experiments were performed in which melting of a phase-change medium occurred in a closed vertical tube which was rotated about a vertical axis colinear with that of the tube. The melting was initiated and maintained by a step-change increase in the wall temperature of the containment tube. During the course of the experiments, parametric variations were made in the rotational speed, in the temperature difference which drives the melting, and in the duration of the melting period. The phase-change medium was 99% pure n-eicosane paraffin with a melting temperature of 36.3 °C. It was found that rotation gave rise to considerably more rapid melting than that for no rotation, with the time required to achieve a given amount of melting being halved due to rotation. The rate at which energy could be stored was also significantly increased by rotation. Furthermore, at any duration of the melting period, the shape of the unmelted solid differed markedly in the presence or absence of rotation, being either straight-sided or sloped-sided. The melted mass results for all of the investigated conditions were very tightly correlated in terms of the Froude, Stefan, Grashof, and Fourier numbers.

INTRODUCTION

MELTING and freezing is an interdisciplinary subject rooted in technologies as diverse as the casting of metals, the processing of foodstuffs, and the storage of thermal energy. Within this diversity of applications, melting and freezing can occur in a wide range of configurations, orientations, and environments. One of the least investigated melting/freezing situations is that in which the phase-change process takes place in the presence of rotation. For melting in the presence of rotation, which is the subject of this paper, there does not appear to be any prior work in the heat transfer literature, as witnessed by the recent surveys reported in refs. [1, 2].

The present research is concerned with melting of a phase-change medium contained in a vertical tube which rotates about a vertical axis that coincides with the axis of the tube. Melting was initiated and sustained when the wall temperature of the containment tube was abruptly raised and maintained at a value which exceeded the phase-change temperature of the medium. The rotation of the tube began at the onset of melting and was maintained at a constant value throughout the melting period. The phase-change medium was 99% pure n-eicosane paraffin (melting temperature 36.3 °C).

Three physical parameters were varied during the course of the experiments. These included the rotational speed (five values), the difference between the temperature of the containment tube and the melting temperature (four values), and the duration of the melting period (as many as nine values). Among the rotational speeds, the case of no rotation was investigated to provide baseline information. In dimensionless terms, the variations of the aforementioned physical parameters gave rise to variations of the Froude number, the Stefan and Grashof numbers, and the Fourier number, respectively. For each data run characterized by preselected values of the rotational speed, the temperature difference, and the melting period, the primary measured quantities were the mass melted during the duration of the run, the bulk temperature of the liquid melt at the end of the run, and the shape of the solid which remained unmelted.

In the presentation of results, the responses of the timewise variation of the melted mass to rotation and to the difference between the tube wall temperature and the melting temperature will be separately highlighted in dimensionless terms. Furthermore, the variation of the melted mass with rotational speed at fixed melting period durations will also be presented, also in terms of dimensionless quantities. To bring together and to generalize the results, a relationship was developed in which a dimensionless melted mass parameter was tightly correlated with the Froude, Stefan, Grashof, and Fourier numbers.

The melted mass measurements yielded information on the energy stored as latent heat during the melting period, while the bulk temperature measurements yielded the energy stored as sensible heat in the liquid melt. These data, taken together, provided the timewise variation of the energy stored as a result of the melting process.

To provide insights into the differences in the melting process with and without rotation, comparisons will be made of the shapes of the unmelted solids resulting from the two modes of melting.

NOMENCLATURE

C	value of M/M_{max} for no rotation	m	*Ste*-dependent exponent, equation (11)
c	specific heat of liquid	R	inner radius of containment tube
E_{max}	maximum value of E_{tot}	*Ste*	Stefan number, $c(T_\infty - T^*)/\lambda$
E_s	sensible energy stored in liquid	T_b	bulk temperature of liquid melt
E_{tot}	stored energy, sum of E_λ and E_s	T^*	melting temperature
E_λ	energy to melt mass M	T_∞	temperature of environment bath
$E_{\lambda,max}$	energy to melt mass M_{max}	t	duration of melting period.
Fo	Fourier number, $\alpha t/R^2$		
Fr	Froude number, $R\omega^2/g$	Greek symbols	
Gr	Grashof number, $g\beta(T_\infty - T^*)R^3/\nu^2$	α	thermal diffusivity of liquid
g	acceleration of gravity	β	thermal expansion coefficient of liquid
M	melted mass	λ	latent heat of melting
M_{max}	mass available for melting	ν	kinematic viscosity of liquid
		ω	rotational speed.

EXPERIMENTS

Apparatus

The vertical containment tube consisted of a cylindrical body fitted with a removable cap at either end. When assembled with the caps in place, the tube had internal dimensions of 1.901 × 19.01 cm, radius × vertical height. The body was a thin-walled brass cylinder (inner radius 1.901 cm, wall thickness 0.297 cm) whose bore was subjected to a succession of finishing operations which culminated in hand-polishing using 600-grit lapping compound. Brass was used because of its relatively high thermal conductivity, its easy machinability, and its compatibility with water (in which the tube was situated during the melting experiments).

The lower end cap was designed to perform two specific functions. One of these was to minimize the heat flow to the bottom of the solid, in keeping with the objective of avoiding thermal end effects. The second was to hold the solid fixed during the melting process so that the axes of the tube and the solid remain colinear.

The end cap was made from Delrin (plastic) rod stock, which was hollowed out to create a cavity to accommodate a 2.54-cm-long cylinder of polystyrene insulation (Styrofoam). The top of the cavity was closed by a thin Delrin disk which formed the lower boundary of the interior of the tube. Integral with the closure disk was a finger-like rod which extended upward into the tube interior. The rod was 3.81 cm long and 0.795 cm in diameter. It was threaded to facilitate intimate bonding with the phase-change medium.

The upper end cap served not only to close the top of the tube but also as the terminus of a shaft which coupled the tube to an electric motor which was the source of rotation. The cap was made of brass for strength, and for the same reason the coupling shaft was machined integral with the cap. A fixture was provided at the upper end of the coupling shaft to facilitate its rapid interconnection to the shaft of the motor.

To avoid heat flow between the upper end cap and the phase-change medium, an air gap was left between the top of the medium and the cap. The air gap also served to accommodate the expansion which occurred during melting and during the subsequent increase in temperature of the liquid melt. The height of the air gap was set with the phase-change medium in the solid state prior to the melting period, the setting being made such that the tube would be completely filled if the solid were to be totally melted and heated to the tube wall temperature. To provide an escape path for the air displaced from the gap due to the expansion of the phase-change medium, a 0.1-cm-diameter vent tube, extending upward 6.4 cm from the upper end cap, was provided.

Two constant-temperature water baths used in the execution of the experiments. One of these, the equilibration bath, was employed to bring the solid phase-change medium to a preselected uniform temperature prior to the initiation of melting. It was equipped with a temperature controller/circulator unit which was set in accordance with the readings of a calibrated chromel–constantan thermocouple immersed in the water.

The second water bath served to establish the thermal environment of the containment tube during the melting period. It was highly agitated to provide high values of the heat transfer coefficient between the water and the outside surface of the tube. The preselected bath temperature was achieved to within 0.05 °C by setting a temperature controller and reading the e.m.f. from an immersed thermocouple. The variable speed motor used to rotate the containment tube overhung the opening of the water bath, with the shaft of the motor pointing vertically downward. The maximum rotational speed provided by the motor with the containment tube in place in the water bath was 260 r.p.m. During the course of the research,

experiments were performed for 0, 70, 140, 210, and 260 r.p.m. As noted earlier, the motor shaft supported the containment tube. Precise vertical positioning was achieved by aligning a scribed line on the body of the tube with a plumb line.

In both of the water baths, the containment tube was positioned so that the air-escape vent tube protruded above the surface of the water.

With regard to instrumentation, mention has already been made of the thermocouples used to monitor the temperatures of the constant temperature baths. The temperature of the containment tube was measured by four thermocouples installed in the cylindrical wall, with the junctions positioned within 0.15 cm of the inner surface of the wall. Measurements of the tube wall temperature were made only for the non-rotating case, since there were no provisions for transmitting the e.m.f.s in the presence of rotation. These measurements established the rapidity with which the tube wall responded to the temperature of the test environment bath.

Another pair of thermocouples was used for the measurement of the bulk temperature of the liquid melt at the preselected termination of the melting period. For this purpose, the two thermocouples were attached to a 0.3-cm-diameter, 30-cm-long nylon stirring rod. The two junctions were located approximately 3.8 cm from one another along the length of the rod.

The thermocouple voltages were read and recorded by a programmable datalogger to 1 μV. The analogue-to-digital clock of the datalogger was used for time-keeping during the experiments.

The measurements of the mass of the paraffin were performed with a triple-beam balance having a capacity of 2610 g and a resolution of 0.1 g. The rate of rotation of the motor shaft was measured by a digital tachometer which resolved to 1 r.p.m. A dial-gage-equipped caliper with a resolution of 0.001 in. was used to quantify the shape of the solid which remained unmelted at the termination of the melting period.

Experimental procedure

Each data run was characterized by preselected values of three parameters: the rotational speed, the temperature of the thermal environment bath in which the containment tube was situated during the melting period, and the duration of the melting period. The time history of the melting process for a given rotational speed and environment bath temperature was determined from a sequence of data runs having successively longer melting periods.

The preparations for a data run were begun with the containment tube free of any vestige of the n-eicosane phase-change medium. Then, with the tube vertical, the paraffin in molten form was poured in through the open top, the pouring and subsequent preparatory operations being facilitated by the attachment of a 5.08-cm-long cylindrical extension at the upper end of the tube. After the filling had been completed, the paraffin was frozen by immersion of the containment tube in an ice bath. Void formation was avoided by establishing a freezing pattern which proceeded from the bottom up. This pattern was achieved by irradiating the upper surface of the paraffin with a low-intensity heat lamp.

After complete freezing had occurred, the upper surface of the paraffin was flattened by successive insertions of a heated disk which was equipped with a guide to ensure that the thus-produced surface was perpendicular to the axis of the tube. The guide also served to fix the height of the gap between the top of the solid paraffin and the upper end cap. The criterion for the selection of the gap height was discussed earlier. After the completion of the flattening operation, the nominal heights of the solid paraffin and of the gap were 17.15 and 1.86 cm, respectively.

The thus-charged containment tube was weighed, after which it was placed in the equilibration bath. The bath temperature was set at 36.0 °C, slightly less than the nominal 36.3 °C melting temperature of the paraffin. Although supplementary experiments had indicated that the paraffin and the tube attained a steady, uniform temperature after 4 h of immersion in the bath, an equilibration period of 8–12 h was generally allowed.

During the later stages of the equilibration period, the thermal environment bath was readied. The temperature of the water was maintained at the preselected value, and the speed control for the motor which served as the source of rotation was set. Immediately preceding the initiation of the melting period, the motor was warmed up.

The containment tube was then transferred from the equilibration bath to the environment bath and coupled to the shaft of the motor, at which point rotation was initiated. These operations were accomplished in about 5 s. During the melting period, the rotational speed and the temperature of the environment bath were monitored periodically and adjusted if necessary. At the preselected termination of the melting period, the containment tube was decoupled from the motor shaft and the air-escape vent tube was sealed.

The tube was then inverted and placed on a bench stand. The lower end cap (now facing up) and the attached unmelted solid were immediately removed, and the thermocouple-equipped nylon stirring rod was introduced through the open end of the tube into the liquid melt. With well-practiced vigorous stirring, the rod-attached thermocouples attained equal, steady values in about 20–30 s, as displayed by the datalogger.

The unmelted solid paraffin, still attached to the end cap, was then weighed. Next, the solid was removed from the cap and marked as to the axial stations at which the diameter was to be measured. At each such axial station, diameter measurements

were made at several circumferential positions with the dial-gage-equipped caliper. The overall length of the solid was also measured.

DATA REDUCTION

The amount of mass liquified between the onset of melting ($t = 0$) and any time t will be denoted by M. It was determined from the aforementioned mass measurements in conjunction with the precisely known masses of the components of the containment tube. To achieve a dimensionless presentation, M will be ratioed with M_{max}, which is the total amount of mass available for melting.

The amount of energy E_λ that is transferred from the tube wall in order to melt the mass M is

$$E_\lambda = \lambda M \tag{1}$$

where λ is the latent heat of melting. Furthermore, to melt the entire solid, the required energy input $E_{\lambda,\,max}$ is equal to λM_{max}. From this, it follows that

$$E_\lambda / E_{\lambda,\,max} = M/M_{max}. \tag{2}$$

Thus, the subsequent presentation of results for M/M_{max} applies equally to $E_\lambda/E_{\lambda,\,max}$.

Each element of the mass M, when first liquified, is at the melting temperature T^*. At the end of the data run, the mass M is at the measured bulk temperature T_b. Therefore, the energy E_s transferred from the tube wall in order to supply the sensible heat stored in the liquid between $t = 0$ and t is

$$E_s = M\int_{T^*}^{T_b} c\,dT. \tag{3}$$

The specific heat c of liquid n-eicosane is well represented by a linear function of temperature [3], so that equation (3) can be readily integrated.

The energy stored in the phase-change medium between $t = 0$ and t, to be denoted by E_{tot}, is the sum of the latent and sensible energy components, i.e.

$$E_{tot} = E_\lambda + E_s = M\left[\lambda + \int_{T^*}^{T_b} c\,dT\right]. \tag{4}$$

The maximum amount of energy E_{max} that can be stored corresponds to the situation in which complete melting has occurred and in which the liquid melt has been heated to the temperature T_∞ of the environment; correspondingly

$$E_{max} = M_{max}\left[\lambda + \int_{T^*}^{T_\infty} c\,dT\right]. \tag{5}$$

It is evident that E_{tot} will approach E_{max} at sufficiently large times. The timewise variations of E_{tot}/E_{max} will be presented later.

As noted earlier, the results will be parameterized by four dimensionless groups, which are, respectively, the Froude number Fr, the Stefan number Ste, the Grashof number Gr, and the Fourier number Fo. The Froude number reflects the rotational speed; the Stefan number serves as a dimensionless temperature difference and also provides a measure of the stored sensible energy; the Grashof number is an index of the vigor of the gravity-induced natural convection; and the Fourier number is a dimensionless time. These quantities were evaluated from their definitions

$$Fr = R\omega^2/g \tag{6}$$

$$Ste = c(T_\infty - T^*)/\lambda \tag{7}$$

$$Gr = g\beta(T_\infty - T^*)R^3/\nu^2 \tag{8}$$

$$Fo = \alpha t/R^2. \tag{9}$$

All the thermophysical properties of the liquid melt which appear in these equations were taken from ref. [3] and evaluated at the melting temperature T^*. The choice of T^* as the reference temperature was motivated by the realization that the thermal resistance at the solid–liquid interface, where T^* prevails, is greater than that at the tube wall (because of the smaller surface area of the interface). The tube inner radius R was chosen as the characteristic dimension of the problem because it better reflects the path length for thermal transfer than does the other candidate characteristic dimension—the height.

It may also be noted that the environment temperature T_∞ has been used in the definitions of Ste and Gr, a choice dictated by the fact that T_∞ was readily measurable while the tube wall temperature could not be measured in the presence of rotation. In view of the high values of the convective heat transfer coefficient at the external surface of the containment tube, T_∞ is very nearly equal to the wall temperature.

Listings of the thermal and rotational parameters of the experiments are presented in Tables 1 and 2, respectively. As seen there, the environment temperature T_∞ was increased in uniform increments, giving rise to uniform-increment changes in Ste and Gr. The rotational speed was also changed in nearly uniform increments.

PATTERNS OF MELTING

The timewise progression of the melting process is illustrated in Figs. 1 and 2. Each figure corresponds to a fixed value of the temperature difference $(T_\infty - T^*)$ which drives the melting, respectively the lowest and highest among those investigated. In dimensionless terms, Fig. 1 is for $Ste = 0.062$ and Fig. 2 is for $Ste = 0.248$.

Table 1. Thermal parameters

T_∞(°C)	$T_\infty - T^*$(°C)	*Ste*	*Gr*
43.24	6.94	0.062	12,270
50.19	13.89	0.124	24,540
57.13	20.83	0.186	36,810
64.07	27.77	0.248	49,080

Table 2. Rotation parameters

ω(r.p.m.)	*Fr*
0	0
70	0.104
140	0.416
210	0.936
260	1.435

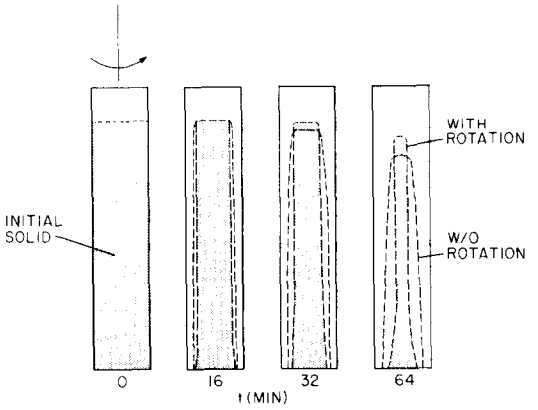

FIG. 1. Timewise progression of the melting process, *Ste* = 0.062.

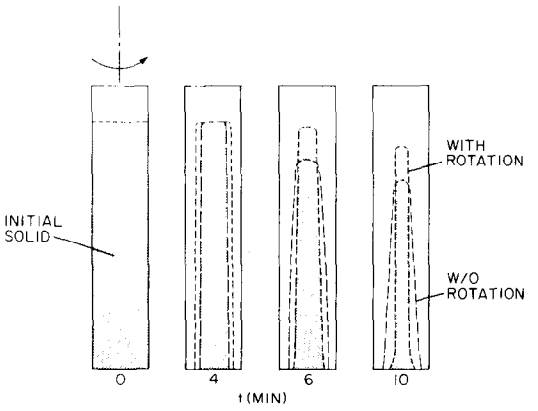

FIG. 2. Timewise progression of the melting process, *Ste* = 0.248.

In each figure, there are four panels which show the shapes of the unmelted solid at various times during the melting process, starting at $t = 0$ at the left and proceeding to larger times from left to right. It may be noted that the melting period durations are substantially greater in Fig. 1 than in Fig. 2, reflecting the slower melting which occurs in the presence of smaller values of $(T_\infty - T^*)$. The vertical rectangle which outlines each panel depicts the boundary of the containment tube.

In each panel, the speckled region represents the unmelted solid corresponding to melting at the highest investigated rotational speed ($\omega = 260$ r.p.m., $Fr = 1.44$). The space contained within the dashed line is the unmelted solid for the no-rotation case ($\omega = Fr = 0$). In the $t = 0$ panel, which shows the pre-melting configuration of the containment tube and the paraffin, the solids for the with-rotation and no-rotation cases, are, of course, coincident. The space between the top of the solid and the containment tube boundary in the $t = 0$ panel depicts the air gap that was discussed earlier.

Inspection of Figs. 1 and 2 reveals significant differences between the with-rotation and no-rotation melting patterns. At any given melting period duration, there is less unmelted solid in the presence of rotation, indicating a higher rate of melting. Furthermore, the unmelted solid for the with-rotation case is generally straight-sided, except near its base. The straight-sidedness reflects spatially uniform melting and a spatially uniform heat transfer coefficient. In contrast, the unmelted solid for the no-rotation case has sloping sides, with the diameter of the solid increasing from top to bottom. This shape is indicative of greater melting and higher heat transfer coefficients at the top than at the bottom.

The melting pattern for the no-rotation case is already well understood [4]. It is primarily a manifestation of a natural convection circulation loop in the liquid melt, with the upflow leg of the loop situated adjacent to the wall of the containment tube and the downflow leg adjacent to the solid–liquid interface. The upflow leg delivers relatively hot liquid to the upper regions of the tube, which accelerates melting there. For the downflow leg, the heat transfer coefficients decrease in the direction from top to bottom. These factors give rise to the shapes of the unmelted solid in evidence in Figs. 1 and 2.

For the with-rotation case, the spatially uniform melting can be rationalized by envisioning a rotation-related breakup of the aforementioned global circulation loop into numerous small circulation loops stacked one atop the other in the annulus between the melting solid and the tube wall. Indeed, the approximate analysis performed in ref. [5] shows such a fluid flow pattern. The departure from spatial uniformity in evidence in Figs. 1 and 2 in the lower portion of the tube may be attributed to the inhibition of the fluid flow due to the bottom corner region.

MELTED MASS

Representative results for the timewise variation of the melted mass are presented in Figs. 3 and 4. Each figure corresponds to a fixed *Ste* (i.e. a fixed temperature difference), respectively *Ste* = 0.124 for Fig. 3 and *Ste* = 0.248 for Fig. 4. Corresponding

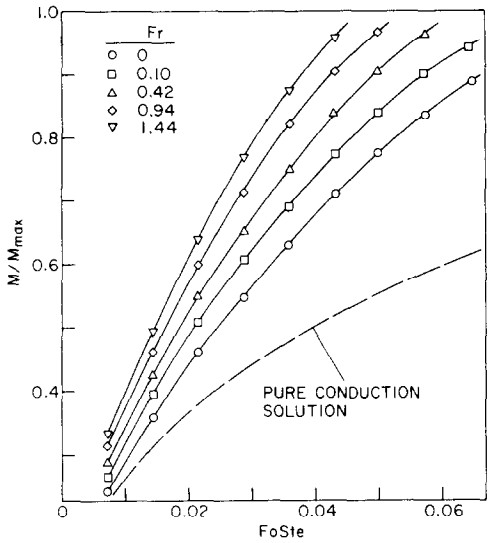

FIG. 3. Timewise variation of the melted mass for parametric values of the rotational speed, $Ste = 0.124$.

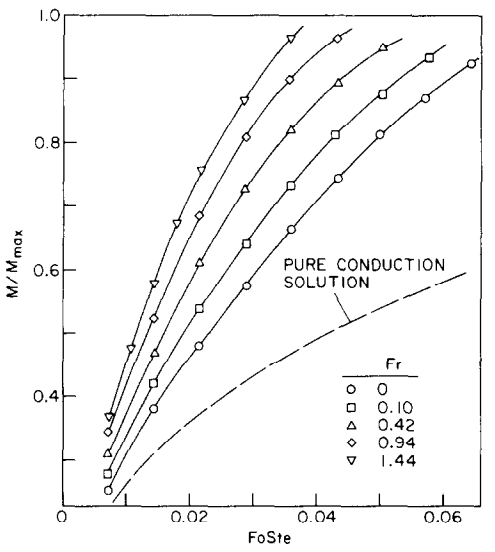

FIG. 4. Timewise variation of the melted mass for parametric values of the rotational speed, $Ste = 0.248$.

results for $Ste = 0.062$ and 0.186 are available in ref. [5].

In each figure, the dimensionless melted mass M/M_{max} is plotted against the $Fo\ Ste$ product, which is a dimensionless time suggested by heat conduction theory. Each figure conveys five sets of experimental results parameterized by the rotational speed expressed in terms of the Froude number. These include the no-rotation case ($Fr = 0$) and four with-rotation cases with Froude numbers ranging from 0.10 to 1.44. For continuity, smooth curves have been passed through the data for each Froude number. In addition to the experimental data, there is included, for reference purposes, a dashed line which represents a numerical solution for melting under conditions where pure conduction is the only mode of heat transfer.

An overview of Figs. 3 and 4 shows that rotation gives rise to a substantial acceleration of melting. For example, for $Ste = 0.124$ (Fig. 3), $M/M_{max} = 0.5$ is achieved at $Fo\ Ste = 0.0145$ for rotation at $Fr = 1.44$, but not until $Fo\ Ste = 0.0245$ in the absence of rotation. The corresponding comparison of the $Fo\ Ste$ values at $M/M_{max} = 0.75$ is 0.0275 and 0.0475. Similar comparisons at $Ste = 0.248$ (Fig. 4) yield $Fo\ Ste$ values of 0.0115 and 0.023 for $M/M_{max} = 0.5$, and 0.0215 and 0.044 for $M/M_{max} = 0.75$. Even for a substantially lower rotational speed such as $Fr = 0.42$, rotation still gives rise to a significant acceleration of melting. These results indicate that rotation provides a viable means for increasing the rate of melting and also that the use of information for no-rotation melting to predict melting in the presence of rotation is conservative.

A comparison of the pure conduction solution and the experimental data for the no-rotation case provides information on the effect of liquid-phase natural convection on the rate of melting. As is already well established, the presence of natural convection increases the amount of melting. At early times, when conduction is the dominant mode of heat transfer, the experimental data are only slightly higher than the pure conduction solution. However, as time proceeds, natural convection takes over, and the deviation of the data from the conduction curve increases—up to 45% in Fig. 3 and 55% in Fig. 4.

As expected, the melted mass increases with time for all of the cases dealt with in the figures, as well as the other cases for which results are conveyed in ref. [5]. The slopes of the M/M_{max} vs $Fo\ Ste$ distributions, which correspond to the rate of melting, decrease as time proceeds. This decrease is believed due to the diminution of the surface area of the unmelted solid which accompanies the melting process.

The experimental results of Figs. 3 and 4, together with similar results of ref. [5] for $Ste = 0.062$ and 0.186, are presented in an alternative perspective in Figs. 5 and 6, where the focus is on the effect of the Stefan number. Each of the figures corresponds to a fixed rotational speed, respectively $Fr = 0$ and 1.44 (no rotation and the largest rotation among those investigated). In each figure, M/M_{max} is plotted vs $Fo\ Ste$ for parametric values of Ste. The curves appearing in these figures are those which were passed through the data in Figs. 3 and 4 plus those passed through the data for $Ste = 0.062$ and 0.186 [5]. The actual data are not shown in Figs. 5 and 6 because, in part, they have already appeared in the preceding figures.

To provide background on the Stefan number effect, it may be noted that for the pure conduction case, the M/M_{max} vs $Fo\ Ste$ distribution is a weak function of the Stefan number in the investigated range. For example, at $Fo\ Ste = 0.05$, $M/M_{max} = 0.553$ for $Ste = 0.062$ while $M/M_{max} = 0.538$ for $Ste = 0.248$. Thus, for pure conduction, M/M_{max} decreases very

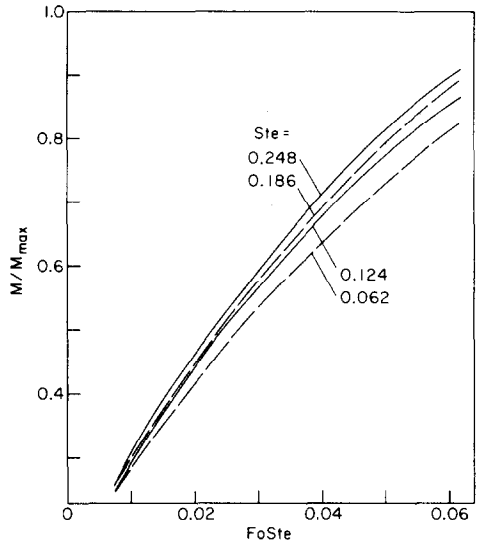

FIG. 5. Timewise variation of the melted mass for parametric values of the Stefan number, $Fr = 0$.

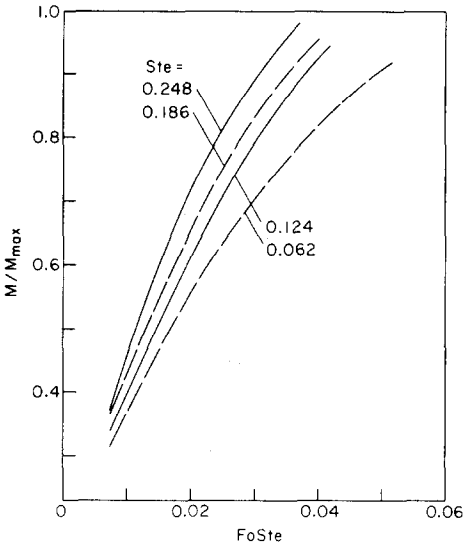

FIG. 6. Timewise variation of the melted mass for parametric values of the Stefan number, $Fr = 1.44$.

slightly with increasing *Ste* at a fixed value of *Fo Ste*. The decrease can be attributed to *Ste*-related sensible heat effects.

Attention will now be turned to Fig. 5, which corresponds to the no-rotation case. Here, the M/M_{max} vs *Fo Ste* distributions show greater sensitivity to *Ste* than for the pure conduction case and, furthermore, M/M_{max} increases with *Ste* at a fixed *Fo Ste*. To rationalize this finding, it may be noted that in this case, *Ste* serves more as an index of the strength of the natural convection than as a measure of the sensible heat absorption. The larger the value of *Ste*, the more vigorous is the natural convection, and the greater is the amount of melting as reflected by M/M_{max}.

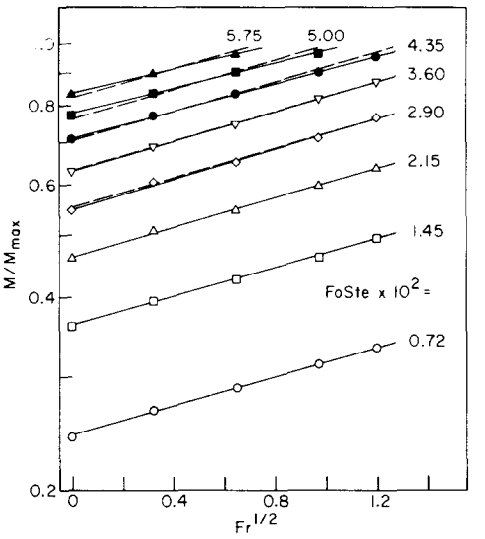

FIG. 7 Dependence of the melted mass on the rotational speed, $Ste = 0.124$.

In Fig. 6, which corresponds to the largest rotational speed, the sensitivity to *Ste* is seen to be further heightened and the trend of M/M_{max} increasing with *Ste* is continued. The greater sensitivity is believed due to the increase of the rotation-induced buoyancy with the temperature difference $(T_\infty - T^*)$ which is embedded in *Ste*.

Although the enhancing effect of rotation on melting was clearly established in Figs. 3 and 4, the presentation format used there does not facilitate the quantitative representation of the effect. Figures 7 and 8, which are the counterparts of Figs. 3 and 4, have been prepared to aid in the development of such a representation. Each figure is a semi-logarithmic plot of M/M_{max} vs $Fr^{1/2}$ (note that $Fr^{1/2} \sim \omega$), with the dimensionless time *Fo Ste* as the data parameter.

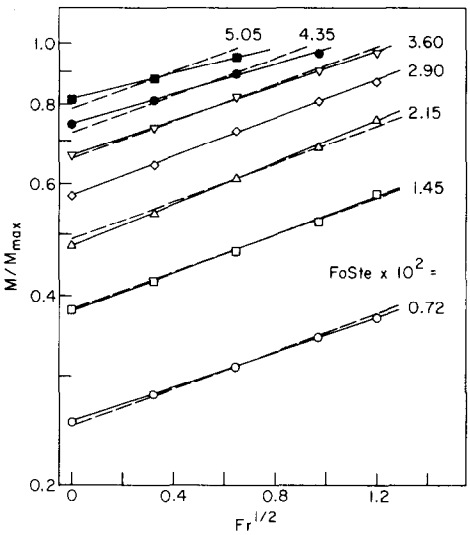

FIG. 8. Dependence of the melted mass on the rotational speed, $Ste = 0.248$.

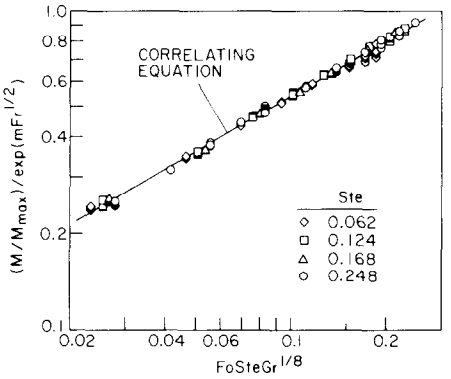

FIG. 9. Correlation of the melted mass results.

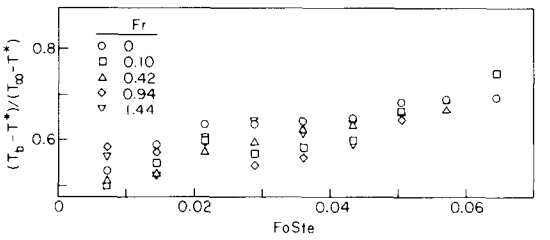

FIG. 10. Representative results for the liquid bulk temperature, $Ste = 0.124$.

As can be seen from these figures, the data corresponding to each parametric value of *Fo Ste* are very well represented by a straight line, indicating that M/M_{max} increases exponentially with the rotational speed, i.e.

$$M/M_{max} = C[\exp(mFr^{1/2})] \quad (10)$$

where m and C are related to the slope and the intercept of each straight line, respectively. The solid lines passed through the data in Figs. 7 and 8 are least-squares fits.

In each figure (i.e. for a fixed *Ste*), the lines for the various *Fo Ste* are virtually parallel, so that their slopes m are nearly equal. This finding motivated a search for a single value of the slope (i.e. of m) which would serve, with minimal errors, for all *Fo Ste* at a given *Ste*. The dashed lines in each figure represent the best common slope for each *Ste*. The greatest deviations between the dashed and solid lines occur at large *Fo Ste*, where the melting is nearly complete. The respective m values for the four investigated *Ste* were correlated by the linear relation

$$m = 0.2 + 0.56Ste \quad (11)$$

with the maximum deviation being 0.76%.

Taking into account the effects of rotation on the melted mass via the $\exp(mFr^{1/2})$ factor, with m given by equation (11), opens the way to a complete correlation of the experimental data. The quantity C in equation (10) is the no-rotation value of M/M_{max} which, based on guidance from the literature, was correlated with *Fo Ste* Gr^n. Here, $n = 1/8$ was found to give the best representation of the data.

To exhibit the final correlation, $(M/M_{max})/\exp(mFr^{1/2})$ is plotted as a function of *Fo Ste* $Gr^{1/8}$ in Fig. 9. The figure contains all of the data that were collected during the melting experiments, although many of the individual data points are obscured by overlap. Also included in the figure is a straight line which represents a least-squares fit of the data, the equation of which is

$$M/M_{max} = 2.05[\exp(mFr^{1/2})(Fo\,Ste\,Gr^{1/8})^{0.58} \quad (12)$$

where m is given by equation (11). The excellence of the correlation is evidenced by the fact that 74% of the data fall within 2% of the correlating line and 98% of the data fall within 5% of the line. The maximum deviation is about 7.8%. Equation (12) accomplishes the generalization which was one of the primary objectives of the research.

STORED ENERGY

As noted earlier, the energy stored in the phase-change medium is the sum of the latent and sensible energy components E_λ and E_s. The latent energy component follows from the already conveyed information for M/M_{max}, since $E_\lambda = \lambda M_{max}(M/M_{max})$. The evaluation of the sensible energy E_s requires a knowledge of the bulk temperature T_b of the liquid melt. Representative results for the measured bulk temperature are presented in Fig. 10, which corresponds to $Ste = 0.124$. In the figure, the bulk temperature appears in a dimensionless ratio on the ordinate, while the abscissa is the *Fo Ste* dimensionless time. The data are parameterized by the rotational speed.

As seen in the figure, there does not appear to be a systematic ordering of the data with the rotational speed. With the data for all rotational speeds considered as a whole, the bulk temperature is seen to increase gradually with time. The extent of the increase is the net result of two conflicting processes. One of these is the heat addition to the liquid at the tube wall, which tends to increase the bulk temperature. The other is the addition of freshly created liquid (having temperature T^*) at the solid–liquid interface, which tends to decrease the bulk temperature. It would be expected that the increase of the bulk temperature would be accelerated following the completion of melting.

The energy E_{tot} ($= E_\lambda + E_s$) stored between $t = 0$ and t is compared with the maximum possible stored energy E_{max} in Figs. 11 and 12, which correspond respectively to $Ste = 0.124$ and 0.248. The E_{tot}/E_{max} ratio is plotted as a function of *Fo Ste* for parametric values of the rotational speed. In interpreting the results, it is relevant to note that each figure is characterized by a single value of E_{max}. Thus, comparisons of E_{tot}/E_{max} within a given figure are tantamount to comparisons of E_{tot}.

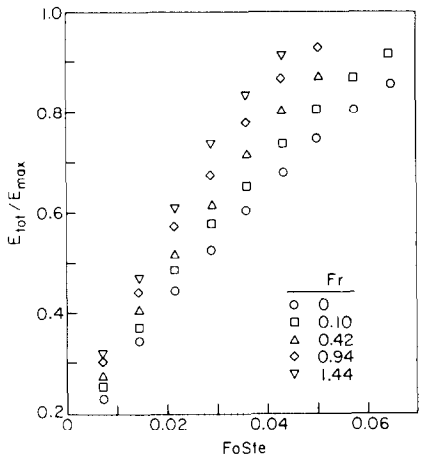

FIG. 11. Timewise variation of the stored energy, $Ste = 0.124$.

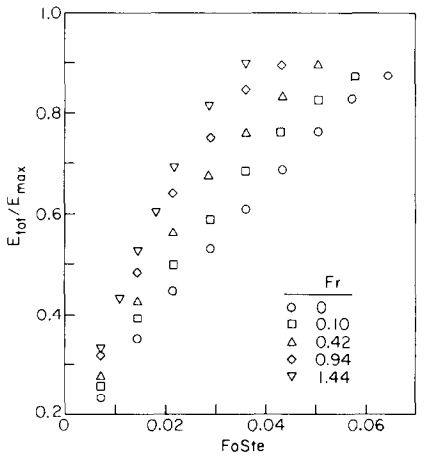

FIG. 12. Timewise variation of the stored energy, $Ste = 0.248$.

The figures show that the presence of rotation enables energy to be stored much more rapidly than when there is no rotation. From Fig. 11 ($Ste = 0.124$), it is seen that $E_{tot}/E_{max} = 0.5$ is achieved at $Fo\ Ste = 0.016$ when $Fr = 1.44$, but not until $Fo\ Ste = 0.0265$ for the no-rotation case. For the $E_{tot}/E_{max} = 0.75$ condition, $Fo\ Ste = 0.03$ for $Fr = 1.44$ and 0.05 for no rotation. In Fig. 12 ($Ste = 0.248$), the corresponding comparisons yield $Fo\ Ste = 0.0135$ and 0.026 at $E_{tot}/E_{max} = 0.5$, and $Fo\ Ste = 0.0245$ and 0.049 for $E_{tot}/E_{max} = 0.75$. These numerical illustrations indicate that if rapid energy transfer is a key objective of a thermal storage system, rotation appears to be a viable option.

The E_{tot}/E_{max} distributions of Figs. 11 and 12 are quite similar in form to those of M/M_{max} in Figs. 3 and 4. This is because the latent heat contribution to E_{tot} substantially exceeds the sensible heat contribution, especially at small Ste.

CONCLUDING REMARKS

Experiments have been performed here to study the effect of rotation on melting of a phase-change medium contained in a closed circular tube. The melting occurred with the tube positioned vertically and with the axis of rotation also vertical and colinear with that of the tube. Prior to the onset of melting, the solid phase-change medium was at a uniform temperature just below the melting temperature. To initiate and maintain the melting, the tube wall was subjected to a step-change increase in temperature. The phase-change medium used in the experiments was 99% pure n-eicosane paraffin with a melting temperature of 36.3 °C.

During the course of the experiments, the rotational speed was varied in five steps from 0 (no rotation) to a maximum value corresponding to a Froude number of 1.44. The thermal driving force for melting was expressed in terms of the Stefan number, which was varied from 0.062 to 0.248 in four steps. This variation of the temperature difference gave rise to a variation of the Grashof number (based on the tube radius) from 12,270 to 49,080. The dimensionless duration of the melting period, expressed as the product of the Fourier and Stefan numbers, ranged from 0.007 to 0.065 in as many as nine steps.

It was found that much more rapid melting was achieved in the presence of rotation. For example, at the highest investigated rotational speed ($Fr = 1.44$), the time required to achieve a given amount of melting was approximately half that for the no-rotation case. The enhancement of melting due to rotation increased moderately with increasing values of the Stefan number. A practically significant ramification of the rotation-related acceleration of melting is that energy can be stored more rapidly in a rotating phase-change system than in a stationary system.

The timewise variation of the melted mass was correlated in dimensionless form for all of the investigated operating conditions. The correlation, which involves the Froude, Stefan, Grashof, and Fourier numbers, is conveyed by equation (12). Seventy-four percent of the data fall within 2% of the correlating line, while 98% of the data fall within 5% of the line.

The pattern of melting was significantly affected by rotation. At any melting period duration, the unmelted solid for the with-rotation case is generally straight-sided, except near its base. The straight-sidedness reflects spatially uniform heating of the solid and a spatially uniform heat transfer coefficient. On the other hand, the unmelted solid for the no-rotation case has sloping sides, with the diameter increasing from top to bottom. This shape is indicative of greater melting and higher heat transfer coefficients at the top of the solid than at the bottom.

REFERENCES

1. R. Viskanta, Phase-change heat transfer, *Solar Heat Storage: Latent Heat Materials* (edited by G. A. Lane), Chap. 5. CRC Press, Boca Raton, Florida (1983).
2. R. Viskanta, A. G. Bathelt and N. W. Hale, Jr., Latent heat-of-fusion energy storage: experiments on heat transfer during solid–liquid phase change, *Alternative Energy*

Sources III. Solar Energy (edited by T. N. Veziroglu), Vol. 1, pp. 279–304. Hemisphere, Washington, D.C. (1983).
3. E. I. Griggs and W. R. Humphries, A design handbook for phase change thermal control and energy storage devices, NASA Technical Paper 1074 (1977).
4. E. M. Sparrow and J. A. Broadbent, Inward melting in a vertical tube which allows free expansion of the phase-change medium, *J. Heat Transfer* **104**, 309–315 (1982).
5. A. Chaboki, Melting in a cylindrical capsule rotating about a colinear axis, Ph.D. thesis, Department of Mechanical Engineering, University of Minnesota, Minneapolis, Minnesota (1985).

FUSION DANS UN TUBE VERTICAL TOURNANT AUTOUR D'UN AXE VERTICAL COLINEAIRE

Résumé—On étudie expérimentalement la fusion d'un milieu qui se produit dans un tube fermé vertical qui tourne autour d'un axe vertical colinéaire avec celui du tube. La fusion est initiée et maintenue par un accroissement, en échelon de la température de la paroi du tube. Pendant les expériences, on fait varier la vitesse de rotation, la différence de température qui assure la fusion et la durée de la période de fusion. Le milieu à changement de phase est la parafine n-eicosane, à 99% de pureté, avec une température de fusion égale à 36,3°C. On trouve que la rotation provoque une fusion beaucoup plus rapide qu'en non rotation, avec un temps divisé par deux pour obtenir une quantité de liquide donnée. La vitesse à laquelle l'énergie peut être stockée est aussi significativement augmentée par la rotation. De plus, à n'importe quelle époque de la fusion, la forme du solide diffère fortement selon l'absence ou la présence de la rotation, étant soit à frontière rectiligne soit à frontière pentue. La masse fondue, pour toutes les conditions étudiées, est reliée de façon nette aux nombres de Froude, Stefan, Grashof et Fourier.

SCHMELZVORGÄNGE IN EINEM SENKRECHTEN ROHR BEI ROTATION UM EINE SENKRECHTE ACHSE

Zusammenfassung—Es wurden Untersuchungen über das Schmelzverhalten in einem geschlossenen, senkrechten Rohr durchgeführt, welches um eine zur Rohrachse parallele Achse rotiert. Durch schrittweises Erhöhen der Rohrwandtemperatur wurde der Schmelzbeginn eingeleitet und das weitere Schmelzen aufrechterhalten. Bei den Versuchen wurden die Rotationsgeschwindigkeit, die Temperaturdifferenz zwischen Wand und Schmelze und die Dauer des Schmelzvorganges variiert. Als Medium wurde das Paraffin n-Eikosan (Reinheit 99%) mit einer Schmelztemperatur von 36,3°C verwendet. Es ergab sich, daß die Rotation zu einer beträchtlichen Erhöhung der Schmelzgeschwindigkeit führt, bis hin zu einer Halbierung der Schmelzdauer. Ebenso erhöhte sich der Betrag der gespeicherten Energie beträchtlich bei der Rotation. Außerdem hat die Rotation zu jeder Zeit einen Einfluß auf die Form des noch nicht geschmolzenen Restes an Schmelzgut. Die Ergebnisse für die Schmelzgeschwindigkeit wurden für alle untersuchten Bedingungen mit Froude-, Stefan-, Grashof- und Fourier-Zahlen korreliert.

ПЛАВЛЕНИЕ В ВЕРТИКАЛЬНОЙ ТРУБЕ, ВРАЩАЮЩЕЙСЯ ВОКРУГ ВЕРТИКАЛЬНОЙ КОЛЛИНЕАРНОЙ ОСИ

Аннотация—Проведены эксперименты, в которых плавление среды с фазовым переходом происходит в закрытой вертикальной трубе, вращающейся вокруг вертикальной оси, коллинеарной с осью трубы. Плавление индуцировано и осуществлено ступенчатым увеличением температуры стенки трубы. В ходе экспериментов варьировались скорость вращения, разность температур, вызывающая плавление, а также длительность процесса плавления. Жидкость с фазовым переходом представляла собой 99% чистый парафин с температурой плавления 36,3°C. Найдено, что в случае вращения процесс плавления существенно ускоряется по сравнению со случаем без вращения, причем время, необходимое для получения заданного количества расплава вследствие вращения уменьшается вдвое. Скорость притока энергии при вращении тоже значительно увеличивалась. Более того, при любой продолжительности процесса плавления форма расплавленного твердого тела резко отличается в случаях с вращением и без него, имея либо прямые, либо наклонные стенки. Количество расплава для всех исследуемых условий определяется числами Фруда, Стефана, Грасгофа и Фурье.